

## Superconducting Proximity Effect at the Paramagnetic-Ferromagnetic Transition

T. Kontos,<sup>1,\*</sup> M. Aprili,<sup>1</sup> J. Lesueur,<sup>1,2</sup> X. Grison,<sup>1</sup> and L. Dumoulin<sup>1</sup>

<sup>1</sup>CSNSM-CNRS, Bâtiment 108 Université Paris-Sud, 91405 Orsay, France

<sup>2</sup>ESPCI, 10 rue Vauquelin, 75005 Paris, France

(Received 14 July 2003; revised manuscript received 4 May 2004; published 23 September 2004)

The exchange-enhanced electron-electron interactions at the paramagnetic-ferromagnetic transition were studied experimentally via proximity effect tunneling spectroscopy. By solving the Usadel equations in both the paramagnetic and ferromagnetic states, the electron-spin fluctuation coupling constant and the exchange field are derived from the tunneling spectra.

DOI: 10.1103/PhysRevLett.93.137001

PACS numbers: 74.50.+r

Superconducting quantum coherence can be induced in a normal metal in contact with a superconductor. This so-called proximity effect is presently well understood when the normal metal is weakly interacting. Equilibrium properties in mesoscopic diffusive proximity structures have been studied extensively [1–3]. In particular, the existence of superconducting correlations in the normal metal was revealed by tunneling spectroscopy measurements of the quasiparticle density of states (DOS) [1]. On the other hand, the use of proximity effect tunneling spectroscopy as a very sensitive tool for phonon spectroscopy in metals is well established [4]. The electron-phonon coupling constant of both the normal ( $N$ ) and the superconducting ( $S$ ) part can be obtained by inverting the tunneling spectra [5]. The proximity effect was also used in the past to induce superconductivity in strongly interacting systems, such as Kondo alloys [6]. However, measurements of electron-electron interactions when increasing the impurity concentration were not considered.

Recent developments [7] in the theory of the proximity effect allow us to address the effect of electron-electron interactions in cases where they are not weak and modify strongly superconducting correlations. Here, we show how exchange-enhanced electron-electron correlations affect the superconducting DOS induced in a normal metal. Specifically, the electron-spin fluctuation coupling constant and the exchange field at the paramagnetic-ferromagnetic transition are obtained by fitting the tunneling spectra using proximity effect theory in the so-called “dirty limit.” The DOS was determined experimentally by planar tunneling spectroscopy in Pd thin films with different Ni concentrations so that both the paramagnetic and ferromagnetic regimes could be explored. For comparison, the superconducting DOS of pure Ag, Pt, and Pd were also investigated.

The microscopic mechanism responsible for the proximity effect is the Andreev reflection. When an electron reaches an  $S/N$  interface, it cannot enter into the superconducting region if its energy  $E$  is smaller than the superconducting energy gap  $\Delta$ . It is then backscattered as a hole with energy  $-E$ . The electron and the hole are coherently coupled. Their phase relationship  $\Delta\varphi =$

$2Et/\hbar$ , where  $t$  is the relevant time scale in the normal region, determines the quantum interferences in the normal metal and hence the DOS [7]. This noninteracting electron picture was originally transcribed in the Usadel equations [8]. Actually, the latter formalism can also accommodate any type of electron-electron interaction in principle [9]. The effect of a large Stoner enhancement as well as that of an exchange field are particularly simple to include. Thus, it becomes possible to follow quantitatively the evolution of the superconducting proximity effect in a metal through the paramagnetic-ferromagnetic transition.

In the paramagnetic regime, the  $S/N$  hybrid structure is described in the dirty limit by the following equations [9]:

$$\begin{aligned} \frac{\hbar D_N}{2} \frac{\partial \theta}{\partial x^2} + i(1 + \lambda_{sf})E \sin\theta + \\ 2\Gamma_{AG} \sin\theta \cos\theta + \Delta_N \cos\theta = 0, \\ \Delta_N = 2\pi T \lambda_N \sum_{\omega} \sin\theta. \end{aligned} \quad (1)$$

$D_N$  and  $\lambda_N$  are, respectively, the diffusion constant and the effective electron-electron coupling constant in the normal slab,  $\lambda_{sf}$  is the electron-spin fluctuations renormalization constant and  $\Gamma_{AG}$  is the Abrikosov-Gor'kov (AG) pair-breaking term [10]. The pairing angle  $\theta$  contains all the information about equilibrium properties and the spatially resolved DOS  $N(E, x)$  is found by  $N(E, x) = \text{Re}(\cos\theta)$  [11].

In the ferromagnetic regime, the pairing angle depends on the spin  $\sigma = \pm 1$  of the quasiparticles because of the exchange field  $E_{ex}$  [12]. Equation (1) reads

$$\begin{aligned} \frac{\hbar D_N}{2} \frac{\partial \theta_{\sigma}}{\partial x^2} + i(1 + \lambda_{sf})(E + \sigma E_{ex}) \sin\theta_{\sigma} + \\ 2\Gamma_{AG} \sin\theta_{\sigma} \cos\theta_{\sigma} + \Delta_N \cos\theta_{\sigma} = 0. \end{aligned} \quad (2)$$

The spatially resolved DOS  $N(E, x)$  is deduced from  $N(E, x) = \text{Re}(\cos\theta_{+} + \cos\theta_{-})/2$  [12].

As can be seen from (1) and (2), both the exchange field and the electron-spin fluctuation coupling constant directly affect the quasiparticle energy  $E$ . The latter is

renormalized by spin fluctuations [13,14], just as it is by phonons in strong coupling superconductors when their energy is much larger than  $\Delta$  [14,15]. The exchange field acts as a spin dependent potential. From (1) and (2), one can define the Cooper pair penetration depth  $\xi_F$  as  $\sqrt{\hbar D_N / 2(\Gamma_{AG} + E_{ex})}$ . Note that the bare Coulomb interaction cannot be neglected, so that *a priori* a nonzero negative gap,  $\Delta_N$  [16], must be considered.

We measured the DOS by planar tunneling spectroscopy in counter-electrode–insulator–normal-metal–superconductor (CE-I-N-S) junctions, using the standard four probe technique [5] (see inset of Fig. 1). The structures were fabricated in an ultrahigh vacuum (UHV) system (base pressure  $10^{-9}$  Torr [17]). A thick Al layer of 1500 Å was deposited at room temperature on a Si(100) substrate with a SiO buffer 500 Å thick. The Al layer was oxidized with an O<sub>2</sub> glow discharge (typical plasma pressure  $8 \times 10^{-2}$  mbar). Depending on the oxidation time (several minutes), junction resistances ranged from 10 Ω to 1 kΩ, for a typical area of  $100 \mu\text{m} \times 100 \mu\text{m}$ . The junction size was defined by evaporating two 500 Å SiO layers. After evaporation of a 50 Å normal metal layer, the latter was covered by a Nb layer (500 Å) whose  $T_c$  was typically 8.7 K. Thicknesses were measured with a quartz deposition controller (accuracy 1 Å). The normal metal was either Ag, Pt, Pd, or Pd<sub>1-x</sub>Ni<sub>x</sub>.

Giant paramagnetism is a well-known feature of Pd metal [13] and a few percent of Ni impurities are sufficient to drive it into the ferromagnetic state. We probed the onset of ferromagnetism by the anomalous Hall effect (AHE) [18] on Pd<sub>1-x</sub>Ni<sub>x</sub> thin films deposited on a bare substrate. As shown in the inset of Fig. 2, an anomalous component proportional to the magnetization appeared

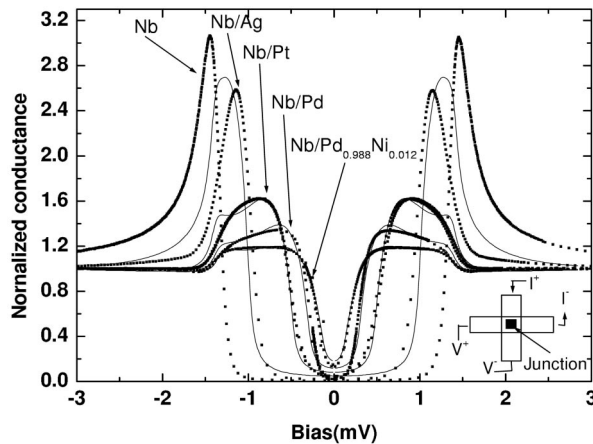


FIG. 1. Measured tunnel conductances (dotted lines) for CE-I-N-S junctions at 300 mK. A finite perpendicular magnetic field of 100 G is used to drive the Al slab into the normal state. The fit (solid lines) with theory is in quantitative agreement with experiment and provides a measure of the electron-spin fluctuation renormalization factor (see Table I). Inset: Junction geometry.

for Ni concentrations higher than 2.4%, just as in bulk Pd<sub>1-x</sub>Ni<sub>x</sub> [19], while hysteresis in the Hall resistivity appeared when  $x \sim 7\%$ , indicating long-range ferromagnetic order. The Ni concentration was determined by Rutherford backscattering spectrometry. Note that the Hall signal was normalized by  $\rho^2$ ,  $\rho$  being the resistivity of the Pd<sub>1-x</sub>Ni<sub>x</sub> thin film, as expected for itinerant ferromagnetism [18].

*The paramagnetic regime.*—Figure 1 shows the tunnel conductance of CE-I-N-S junctions with N being pure Ag, Pt, Pd, and Pd<sub>0.988</sub>Ni<sub>0.012</sub>. The main feature of the conductance is a minigap,  $E_g$ , which is a signature of finite size effects ( $d_N < \xi_F$ ) [11]. Thus, the decay of superconducting correlations in these metals has a typical length scale larger than 50 Å. Note that the minigap decreases when the susceptibility of the metal increases. In Fig. 1, we also show the fit of the conductance to the DOS deduced from the Usadel equations. We used a self-consistent code to solve Eq. (1) together with the usual boundary conditions [20]. It turns out that a finite  $\Delta_N$  is unnecessary to account for the data and that an upper bound for the coupling constant  $\lambda_N$  is  $-0.1$ . The results are given in Table I. A finite interface resistance of about  $5 \times 10^{-4} \mu\Omega \text{cm}^2$  was used to account for both the shape and the value of the energy gap for pure Pd. This value is consistent with that measured in Nb/Pd/Nb Josephson junctions [21]. This finite resistance is assumed not to vary when changing N and also to remain constant when

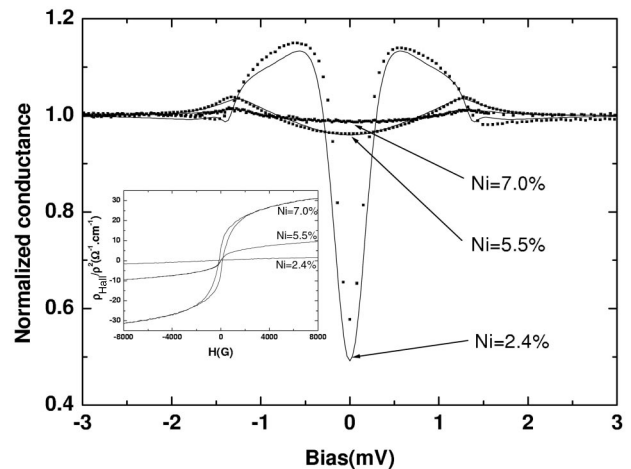


FIG. 2. DOS for Ni concentration for 2.4%, 5.5%, and 7% measured at 300 mK (dotted lines). The thickness of the Pd<sub>1-x</sub>Ni<sub>x</sub> was kept constant, equal to 50 Å. The minigap disappears at the transition between the paramagnetic state and the ferromagnetic state. For concentrations higher than 4.0% the only energy scale is the Nb energy gap. Quantitative fits (solid lines) provide a measurement of the departing energy at Ni concentrations above 2.4% (see Table I). Inset: Onset of ferromagnetic order probed at  $T = 1.5$  K by AHE in 50 Å-thick Pd<sub>1-x</sub>Ni<sub>x</sub>. An anomalous component appears above  $x \sim 2.5\%$  and a hysteresis loop for  $x \sim 7.0\%$ .

TABLE I. Results of the fitting procedure for Ni concentrations from 0% to 11.5%. The first column indicates the normal metal when it differs from  $\text{Pd}_{1-x}\text{Ni}_x$ .

Ni(at. %)	$\rho_{\text{Hall}}/\rho^2$	$\lambda_{\text{sf}}$	$\Gamma_{\text{AG}}(\text{meV})$	$E_{\text{ex}}(\text{meV})$	$\Gamma(\text{meV})$
Ag	0	0.05	0	0	0.05
Pt	0	2.05	0.075	0	0.075
Pd	0	4.15	0.075	0	0.075
1.2	0	5.3	0.20	0	0.20
2.4	0	4.15	0.17	0	0.17
3.2	2.55	4.15	0.4	0	0.4
4.0	7.35	4.15	0.55	0	0.55
5.5	8.65	4.15	0.8	0.11	0.91
6.0	10.25	4.15	1.15	0.45	1.6
7.0	27.5	4.15	1.15	2.80	3.95
9.8	58.0	4.15	1.2	3.26	4.46
11.5	95	4.15	1.25	3.89	5.14

adding Ni impurities to Pd. The electron-spin fluctuation coupling constant increases from Ag to Pt and from Pt to Pd. It further increases when increasing the Ni concentration, as expected since specific heat data [22] show a magnetic susceptibility increase below the paramagnetic-ferromagnetic transition. The exact relationship between  $\lambda_{\text{sf}}$  and Stoner enhancement is model dependent, but a rough estimate is given by  $\lambda_{\text{sf}} \approx 2(1 - 1/S) \ln S$  [14], where  $S$  is the Stoner enhancement. This yields a Stoner enhancement of 10 for Pd, 3.3 for Pt, and 1 for Ag, in surprisingly good agreement with the known values for these metals.

*The ferromagnetic state.*—Figure 2 displays the changes in the DOS when adding Ni impurities in Pd. Note that the number of low lying excitations increases. For 5.5% of Ni, the energy scale of the minigap disappears, suggesting that finite size effects vanish. The AHE magnetization data indicate no long-range order below 5.5% and the induced pair function is small, so that we can fit the data with a non-self-consistent calculation of the DOS by solving (2) with  $E_{\text{ex}} = 0$  and  $\Delta_N = 0$  below 5.5%. The pairing angle  $\theta_0$  in the normal slab and the pairing angle  $\theta_S$  in the superconducting slab at the  $S/N$  interface are solutions of the following equations [7,11,20]:

$$\sin\theta_0(\cos\theta_S - i2\gamma_B E/E_{\text{ThN}}) + \frac{4\gamma_B}{E_{\text{ThN}}} \Gamma_{\text{AG}} \sin\theta_0 \cos\theta_0 - \sin\theta_S \cos\theta_0 = 0, \quad (3)$$

$$(-E^2 + \Delta^2)^{1/4} \sin\left(\frac{\theta_S - \theta_{\text{BCS}}}{2}\right) = \frac{\gamma\sqrt{E_{\text{ThS}}}}{\gamma_B\sqrt{2}} \sin(\theta_0 - \theta_S), \quad (4)$$

where  $\gamma_B = \rho_B \sigma_N / d_N$  and  $\gamma = \sigma_N d_S / \sigma_S d_N$  are the usual boundary parameters.  $E_{\text{ThN(ThS)}} = \hbar d_{N(S)} / d_{N(S)}^2$ ,  $\sigma_{N(S)}$ , and  $d_{N(S)}$  are, respectively, the Thouless energy,

the conductivity, and the thickness of the  $N(S)$  layer.  $\rho_B$  is the interface resistance of the  $S/N$  interface.  $\theta_{\text{BCS}}$  is the pairing angle of a bulk superconductor. As the ratio  $\alpha = \gamma/\gamma_B$  found from the self-consistent code is small ( $\gamma_B = 5.3$  and  $\gamma = 0.1$ ), we can solve Eq. (3) with the ansatz  $\theta_S = \theta_{\text{BCS}} + \delta\theta_S$ , with  $\delta\theta_S \ll 1$ . We find very good agreement with the data, as seen in Fig. 2. Thus, an AG pair-breaking term can account for the tunneling spectra when ferromagnetic order is not yet fully established [23].

For Ni concentrations higher than 5.5%, the tunnel conductance displays only one characteristic energy,  $\Delta$ , of about 1.35 meV, while the shape of the spectra remains roughly the same. This is best seen in Fig. 3, where all the spectra have been scaled to the DOS corresponding to 5.5% of Ni. As finite size effects vanish, the proximity bilayer becomes similar to that of a semi-infinite mesoscopic system ( $d_F > \xi_F$ ). The overall amplitude is smaller than 5% of the background conductance and it is therefore possible to find an analytical expression for the DOS, leading directly to the exchange field value in the  $\text{Pd}_{1-x}\text{Ni}_x$  layer. Linearizing Eq. (2), we find the following DOS:

$$N(E) = 1 + [N_0(E) - 1] \exp\left(-2\sqrt{\frac{E_{\text{ex}}}{E_{\text{ThN}}}}\right) \cos\left(2\sqrt{\frac{E_{\text{ex}}}{E_{\text{ThN}}}}\right), \quad (5)$$

where  $N_0(E)$  is the DOS at the boundary between Nb and  $\text{Pd}_{1-x}\text{Ni}_x$ . Note that  $N_0(E)$  is not universal as it depends on  $\gamma$  and  $\gamma_B$ . Figure 4 displays the depairing energy  $\Gamma$ , defined as  $\Gamma_{\text{AG}} + E_{\text{ex}}$ , as a function of Ni concentration.  $\Gamma$  is constant below 2.5% and it increases for higher con-

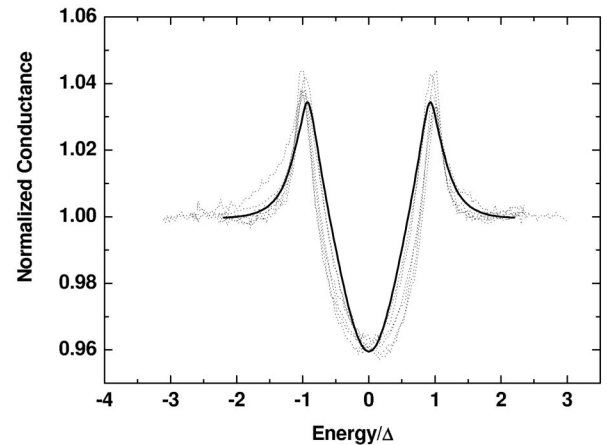


FIG. 3. Densities of states measured in the ferromagnetic state for Ni concentrations above 5.5% at 300 mK (dashed lines). For clarity, the spectra are scaled to that corresponding to 5.5% Ni. Only one characteristic energy scale, the energy gap of Nb  $\Delta$  (about 1.35 meV), is observed, suggesting that finite size effects are irrelevant. The semi-infinite limit for the ferromagnetic layer is recovered. The fit (thick solid line), using the Eq. (5), allows us to deduce the exchange field.

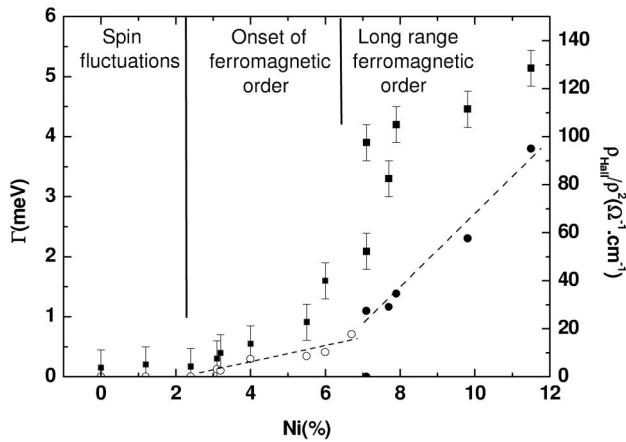


FIG. 4. Measured depairing energy (squares, left axis) as a function of Ni concentration. Three regimes occur. In the spin fluctuation regime, the depairing  $\Gamma$  displays no variation with Ni concentration as long as the latter remains below 2.5%. Ferromagnetism sets in for Ni concentrations above 2.5%, the dominant depairing mechanism then being AG-like. Long-range ferromagnetic order occurs at Ni concentrations above 7%, and hysteresis appears in the Hall signal. The Hall signal increase roughly linearly below 7% (open circles, right axis) and displays an up turn above 7% (solid circles, right axis).

centrations. In the ferromagnetic regime, a jump around 7% occurs, at the transition from AG depairing to an exchange field-dominated depairing mechanism. Figure 4 also displays the saturation magnetization found from the Hall signal (right axis) as a function of Ni concentration. It also increases with the Ni concentration. The kink appearing around 7% Ni concentration corresponds to the appearance of hysteresis in the Hall signal. Modifications in the magnetic domain structure can then affect superconducting correlations, probably due to a change in domain size after long-range ferromagnetic order sets in. Note also that  $\Gamma_{AG}$  saturates to 1.2 meV, suggesting that spin waves are no longer modified in this Ni concentration range.

In summary, we have studied the proximity effect in the vicinity of the paramagnetic/ferromagnetic transition using planar tunneling spectroscopy. The differential conductance of CE-I-N-S junctions, where N is a strongly paramagnetic or a ferromagnetic thin film, allowed a direct measurement of the electron-spin fluctuation coupling constant in the paramagnetic state, and of the exchange field in the ferromagnetic state. For Ni concentrations higher than 5.5%, the DOS shape scales simply by a function of  $E_{ex}/E_{ThN}$ , indicating that finite size effects are irrelevant when the depairing energy is higher than the Nb energy gap.

Finally, we note that proximity effect tunneling spectroscopy may be generalized to investigate other strongly correlated electron systems, such as metals near a quantum critical point.

We acknowledge fruitful discussions with Y. Nazarov, A. Anthore, H. Pothier, D. Estève, and J. Budnick. We thank W. Belzig and H. Bernas for a critical reading of the manuscript.

\*Present address: Institute of Physics, University of Basel, Klingelbergstrasse 82, CH-4056 Basel, Switzerland.

- [1] S. Guéron, H. Pothier, N.O. Birge, D. Estève, and M. Devoret, *Phys. Rev. Lett.* **77**, 3025 (1996).
- [2] P. Charlat, H. Courtois, Ph. Gandit, D. Mailly, A.F. Volkov, and B. Pannetier, *Phys. Rev. Lett.* **77**, 4950 (1996).
- [3] P. Dubos, H. Courtois, B. Pannetier, F.K. Wilhelm, A.D. Zaikin, and G. Schön, *Phys. Rev. B* **63**, 064502 (2001).
- [4] P.M. Chaikin, G.B. Arnold, and P.K. Hansma, *J. Low Temp. Phys.* **26**, 229 (1977).
- [5] E.L. Wolf, *Principles of Electron Tunneling Spectroscopy* (Clarendon Press, New York, 1985).
- [6] L. Dumoulin, E. Guyon, and P. Nedellec, *Phys. Rev. B* **16**, 1086 (1977).
- [7] W. Belzig, Ph.D. thesis, University of Karlsruhe, 1999.
- [8] K.D. Usadel, *Phys. Rev. Lett.* **25**, 507 (1970).
- [9] J.W. Serene and D. Rainer, *Phys. Rep.* **101**, 221 (1983).
- [10] A.A. Abrikosov and L.P. Gor'kov, *Sov. Phys. JETP* **12**, 1243 (1961).
- [11] W. Belzig, C. Bruder, and G. Schön, *Phys. Rev. B* **54**, 9443 (1996).
- [12] Z. Radovic *et al.*, *Phys. Rev. B* **44**, 759 (1991).
- [13] J.M. Daams, B. Mitrovic, and J.P. Carbotte, *Phys. Rev. Lett.* **46**, 65 (1981).
- [14] S.V. Vonsovky, Yu.A. Izyumov, and E.Z. Kurmaev, *Superconductivity in Transition Metals* (Springer-Verlag, Berlin, 1982).
- [15] G.M. Eliashberg, *Sov. Phys. JETP* **11**, 696 (1960).
- [16] Yu.V. Nazarov and T.H. Stoof, *Phys. Rev. Lett.* **76**, 823 (1996).
- [17] T. Kontos, M. Aprili, J. Lesueur, and X. Grison, *Phys. Rev. Lett.* **86**, 304 (2001).
- [18] G. Bergmann, *Phys. Rev. Lett.* **41**, 264 (1978).
- [19] J. Beille, Ph.D. thesis, Université Joseph Fourier, Grenoble, 1975.
- [20] A.A. Golubov and Yu. Kupriyanov, *J. Low Temp. Phys.* **70**, 823 (1988).
- [21] W. Guichard, Ph.D. thesis, Université Joseph Fourier, Grenoble, 2003.
- [22] G. Chouteau, R. Fourneau, R. Tournier, and P. Lederer, *Phys. Rev. Lett.* **21**, 1082 (1968).
- [23] L.P. Gor'kov and A.I. Rusinov, *Sov. Phys. JETP* **19**, 922 (1964).